Journal of Low Temperature Physics
https://doi.org/10.1007/s10909-024-03217-8

Antenna-Coupled Magnetic Microbolometers for CMB Polarization Surveys

Juan Geria[1,2,4] · Alejandro Almela[1,4] · Juan Bonaparte[2,5] · Jesús Bonilla-Neira[1,2] · Luciano Ferreyro[1,3,4] · Alan Fuster[1,4] · Manuel García Redondo[1,3,4] · Matías Hampel[1,4] · Nahuel Müller[1,2,4] · Manuel Platino[1] · Juan Salum[1,3] · Sebastian Kempf[2] · Marc Weber[3] · Alberto Etchegoyen[1]

Received: 3 November 2023 / Accepted: 4 September 2024

Abstract
In this work, we propose a magnetic bolometer to be employed in the search of primordial B-modes in the CMB. These magnetic bolometers are an adaptation of the well-known metallic magnetic calorimeters used in particle physics. They rely on the magnetization dependence on temperature of alloys such as Au:Er and Ag:Er. In addition to the low intrinsic noise a magnetic bolometer of this nature offers, the broad and smooth temperature-dependent magnetization of metallic magnetic sensors ultimately translates to a high dynamic range and straightforward calibration. Their intrinsic noise equivalent power (NEP) is estimated to be in the range of 10–100 aW/$\sqrt{(}$Hz). We outline here a workable design for such a detector utilizing an antenna-coupled approach and present the simulated power transfer ratio that was attained; the detector's performance is discussed by combining this result with its responsivity.

Keywords Magnetic microbolometer · Antenna-coupled bolometer · Magnetic microcalorimeter · CMB

✉ Juan Geria
juan.geria@iteda.cnea.gov.ar

[1] Instituto de Tecnologías en Detección y Astropartículas (ITeDA), Buenos Aires, Argentina

[2] Institute of Micro- and Nanoelectronic Systems (IMS), Karlsruhe Institute of Technology (KIT), Karlsruhe, Germany

[3] Institute of Data Processing and Electronics (IPE), Karlsruhe Institute of Technology (KIT), Karlsruhe, Germany

[4] Universidad Tecnológica Nacional, Buenos Aires, Argentina

[5] Comisión Nacional de Energía Atómica, Buenos Aires, Argentina

Published online: 16 September 2024

1 Introduction

Detection of B-modes in the polarization pattern of the cosmic microwave background (CMB) is considered a direct observation of primordial gravitational waves that took place 10^{-34} s after the Big Bang [1, 2].

Due to the sensitivity required to reliably detect primordial B-modes, low-temperature detectors, e.g., cryogenic bolometers, are required to reduce detection noise to the lowest possible level. The limited space inside typical CMB telescopes demands compact detector arrays for which antenna-coupled multichroic schemes are an attractive approach [3]. State-of-the-art CMB detectors aimed for the detection of B-modes consist of antenna-coupled detectors that use either transition edge sensors (TESs) or microwave kinetic inductance detectors (MKIDs) as the sensing element [4].

In [5], we proposed a new type of sensing element that uses the temperature-dependent magnetic nature of paramagnetic alloys, such as gold–erbium (Au:Er) and silver–erbium (Ag:Er), instead of superconducting films' electric transport characteristics. Magnetic microcalorimeters (MMC) use these sensors to detect high-energy particles [6, 7]. We refer to the resulting detector, which is an adaptation of the well-known MMC, as the magnetic microbolometer (MMB). Simulations presented in [5] show that the proposed MMB can perform background limited photometry (BLIP) with typical restrictions observed on current CMB instruments.

Advantages that this technology offers are lower Johnson noise associated to detector readout due to its dissipationless nature, high dynamic range, straightforward calibration and the ability to achieve a high degree of rejection to external magnetic fields through the use of a gradiometric layout design [8].

In the following sections, a description of the detector architecture is given and the simulated performance is discussed. To extract the essential requirements and ascertain whether the MMB is applicable for CMB B-mode polarization surveys, we use the QUBIC instrument [9] as reference. An analogous examination can be employed to evaluate MMB's suitability in other contexts.

2 Detector Architecture

Figure 1 left displays the detector architecture. A planar polarimetric antenna couples incoming radiation onto a microstrip transmission line. Inline millimeter-wave band-pass filters separate the bands of interest. Each filtered signal is directed to a suspended island weakly coupled to a thermal bath that houses a termination resistor in tight thermal contact with a paramagnetic Au:Er sensor. The sensor is magnetically coupled to a superconducting pick-up coil that simultaneously provides biasing by means of a persistent supercurrent. Excess currents are generated in the pick-up coil as the magnetization of Au:Er sensor changes due to the dissipated power from the termination resistor. The observing bands

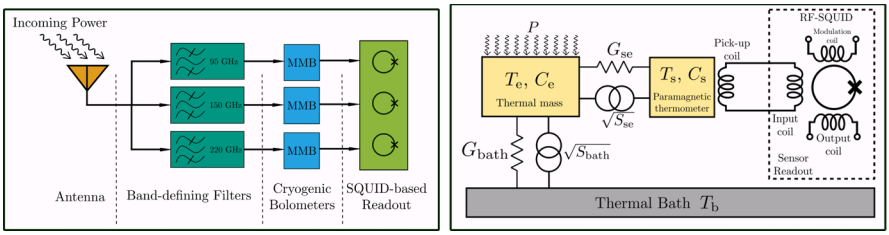

Fig. 1 Left: Schematic representation of the pixel architecture. Right: Thermal model of the MMB. P represents the coupled and filtered incoming power, T_e and T_s are the temperatures of the electron and spin subsystems, C_e and C_s their corresponding heat capacities, G_{bath} is the heat conductance to the thermal bath, and G_{se} is the heat conductance representing electron–spin interactions within the paramagnetic temperature sensor. Thermal fluctuation noise sources are represented for each heat conductance as $\sqrt{S_{\text{bath}}}$ and $\sqrt{S_{\text{se}}}$. The excess current generated at the pick-up coil can be readout and multiplexed using a Microwave SQUID Multiplexer (μMux)

considered in the present work are the central 150 GHz plus a 220 GHz and 95 GHz with 25% of fractional bandwidth.

The signal produced by the MMB can be understood with the thermal model also shown in Fig. 1. Incoming power (P) in this diagram represents the power dissipated by the termination resistor. This power is translated into a temperature variation of the absorber thermal mass that interacts via electron–spin interactions with the immersed spin system within the paramagnetic sensor. The sensor is penetrated by an applied weak magnetic field. The thermal exchange produces fluctuations in the spin system that translate to a measurable magnetization variation, coupled via a flux transformer to a Superconducting QUantum Interference Device (SQUID). For multiplexing of large detector arrays, a Microwave SQUID Multiplexer (μMUX) [10–14] can be used.

3 The Magnetic Microbolometer

In Fig. 2, the detector schematic is presented together with the design layout of the suspended MMB. The detector needs to be biased with a constant weak magnetic field that is produced by a persistent current (I_{field}) circulating through the pick-up coil (L_{m}). A heat switch [15] consisting of a thin-film resistor placed in close proximity to a section of the circuit is used to introduce I_{field} by applying a short current pulse that momentarily suppresses superconductivity by Joule heating. In this design, a load inductor (L_{load}) is included to produce a higher coupling of the SQUID's input inductance (L_{in}) to the signal produced by the sensor. This topology has also been proposed for MMC arrays used in projects such as Lynx [16].

A significant rejection to external magnetic fields can be achieved using a particular geometry for L_{m} [17] in which the leads are symmetrically enclosing a meander-like inductor and form a superconducting loop around it, as shown in Fig. 2. This was confirmed by simulations of the mutual inductance between L_{m} and an external loop. Concerning SQUIDs, gradiometric designs have

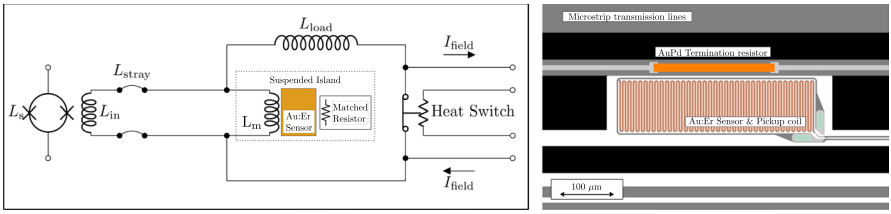

Fig. 2 Left: MMB schematic, the detector is part of two closed superconducting circuits, a biasing loop that helps create a noise-free biasing field and a readout loop that consists of a flux transformer coupled to a SQUID. Right: Suspended MMB layout. Four thin dielectric beams made of silicon nitride hold a rectangular suspended island housing a AuPd termination resistor and thermally coupled Au:Er sensor. Underneath the sensor lies a meander-shaped pick-up coil for bias and readout. This layout corresponds to the section of the schematic on the left labeled "Suspended Island", which is represented by a dashed rectangle

demonstrated external field rejection as well that can be complemented by active feedback techniques [18].

4 Pixel Design

The radiation is coupled to the millimeter-wave circuit via a planar sinuous antenna that is capable of discriminating between orthogonal linear polarizations and presents a broadband response that encompasses the three observing bands. This type of antenna has been extensively employed for multichroic polarization sensitive pixels of several CMB experiments [19–22].

The gaussianity of the antenna's beam is enhanced by the use of hemispherical lenslets made of silicon or materials with similar dielectric constant, also increasing the antenna's gain on bore sight [23]. A Dolph–Chevyshev impedance transformer or taper [24] is implemented to obtain a maximally flat impedance matching of the antenna with the rest of the circuit which has a much lower impedance. The impedance taper is guided through the arms of the antenna.

Inline filters determine the pixel's observation bands. Tubular band-pass filters [25] are implemented using stepped impedance microstrip and CPW lines. This approach was employed by other projects such as POLARBEAR-2 and the Simons Array [26]. Three band-pass filters were designed at frequencies of 95 GHz, 150 GHz, and 220 GHz, having a fractional bandwidth of 25%.

Figure 3 shows the detector's layout. The biasing loop's load inductance is made up of three double-spiral coils positioned around the pixel. In this system, all six MMBs in a pixel can be biased using only two DC pairs: one for the heat switch pulse and one for the field current. This persistent current injection circuit, in principle, permits many pixels to be connected in series, lowering the total number of DC bias lines necessary for large arrays.

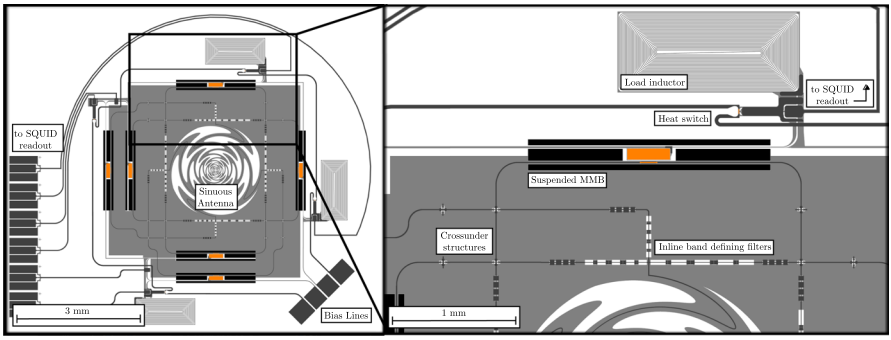

Fig. 3 Conceptual design layout of an antenna-coupled multichroic detector pixel based on a sinuous antenna. A Dolph–Chevyshev taper guides the coupled signal to inline band-pass filters that define the observation bands. The filtered signals are then differentially fed to six suspended MMB detectors placed around the pixel

5 Results

The total pixel power transfer ratio between the antenna and the termination resistors was obtained by combining 3D and 2.5D EM simulations from each microwave component. Plots showing the ratio of incoming to dissipated power spectrum assuming a perfectly matched antenna and also accounting for the simulated antenna impedance can be observed in Fig. 4.

The results show that this multichroic antenna-coupled detector yields a high optical coupling efficiency for multiple observation bands in a single pixel. We see in Fig. 4 right that the coupling efficiency suffers a considerable reduction that can be attributed to the antenna's varying impedance. Further reduction of the coupling efficiency is expected from microfabrication tolerances and artifacts affecting the in line band defining filters and cross-under structures as reported by other groups [27].

To assess the performance of the design, the background and detector noise equivalent power (NEP_{ph} and NEP_{det}, respectively) were calculated. Considering the emissivity, transmittance and spillover losses of the optical components in the QUBIC instrument [28, 29] and in combination with the power transfer ratio shown

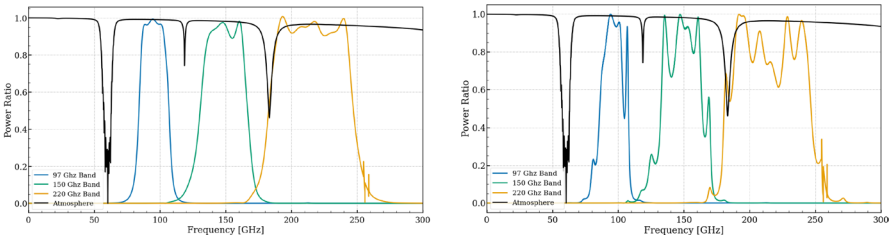

Fig. 4 Left: Pixel response assuming a perfectly matched antenna. Right: Pixel response including the simulated broadband sinuous antenna. Solid black line represents simulated atmospheric transmission, and solid color lines represent the spectral power density absorbed by each suspended bolometer

in Fig. 4 right, a total optical incoming power of 4.91 pW reaches the MMB for the 150 GHz band. Using the equations presented in [30] for diffraction limited single mode detectors, $\mathrm{NEP_{ph}}$ is calculated from the incoming power spectral density to be 45.57 aW/$\sqrt{\mathrm{Hz}}$.

Figure 5 left shows the $\mathrm{NEP_{det}}$ in black solid line assuming a bath temperature of 300 mK considering the base temperature of the QUBIC instrument. The MMB has five known noise contributions listed in the legend of this plot, a description of each of these contributions can be found in [5]. Detector noise contributions are represented in dashed traces. Finally, the estimated $\mathrm{NEP_{ph}}$ is shown in blue solid trace. In the right plot of Fig. 5, the $\mathrm{NEP_{det}}$ for multiple bath temperatures is shown. For the specific instrument under consideration, BLIP can be marginally achieved with the MMB; however, as the plot on the right illustrates, lower bath temperatures result in a lower $\mathrm{NEP_{det}}$ at the expense of a slower response time (τ). These results can be explained as follows: at lower temperatures, the suspending legs have less heat conductance (G), which increases the detector's responsivity at the expense of a larger time constant, $\tau \propto C/G$, where C is the bolometer's heat capacity and remains invariant or may increase as well due to the Schottky anomaly [31]. In addition, the magnetization (M) of the paramagnetic sensor presents a steeper temperature dependence following Curie law ($M \propto 1/T$) also increasing sensitivity and reducing $\mathrm{NEP_{det}}$.

6 Conclusion

We presented the design of a new type of cryogenic detector based on an antenna-coupled multichroic pixel in which a suspended bolometer is implemented using a paramagnetic temperature sensor made of Au:Er to be used in CMB polarization surveys. EM simulations of the pixel design combined with simulations of the MMB responsivity suggest that for a given set of parameters BLIP can be achieved. It is

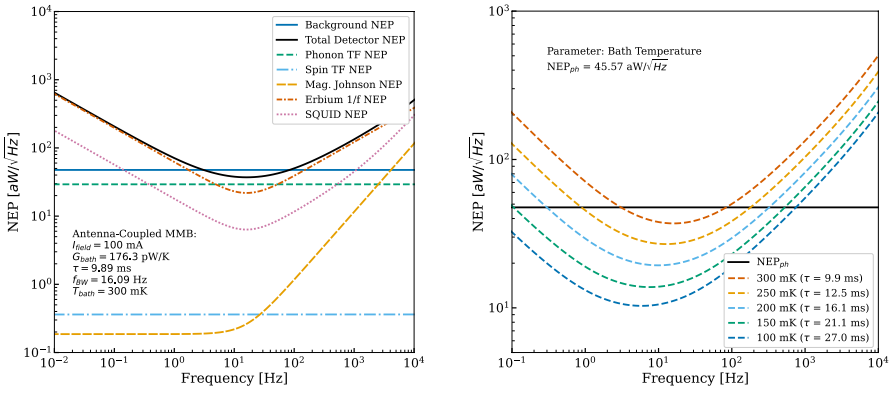

Fig. 5 Left: Total $\mathrm{NEP_{det}}$ compared to estimated $\mathrm{NEP_{ph}}$, the plot also enumerates individual detector noise sources and shows their contribution. Right: $\mathrm{NEP_{det}}$ for multiple bath temperatures with the respective time constants for each case

also shown how lowering the bath temperature improves the detector performance significantly.

Experimental proof of concept of the MMB is the goal of further development. Fabrication and measurements of sensitivity and timing characteristics are currently being pursued. In a further stage of development, an antenna coupling circuit such as the one described in this paper will be used to demonstrate its potential use as a highly sensitive bolometer for astronomic applications. In particular, a dual band variant that is envisioned for the upgrade of the ongoing QUBIC experiment [32].

Acknowledgements Juan Geria is supported by the Consejo Nacional de Investigaciones Científicas y Técnicas (CONICET) as well as the Helmholtz International Research School in Astroparticles and Enabling Technologies (HIRSAP). Juan Geria would also like to acknowledge the support given from the Karlsruhe School of Elementary and Astroparticle Physics: Science and Technology (KSETA).

Funding Open Access funding enabled and organized by Projekt DEAL.

References

1. D.N. Spergel, M. Zaldarriaga, Cmb polarization as a direct test of inflation. Phys. Rev. Lett. (1997). https://doi.org/10.1103/PhysRevLett.79.2180
2. U. Seljak, M. Zaldarriaga, Signature of gravity waves in the polarization of the microwave background. Phys. Rev. Lett. **78**(11), 2054–2057 (1997). https://doi.org/10.1103/PhysRevLett.78.2054. arXiv:9609169
3. A. Suzuki, K. Arnold, J. Edwards, G. Engargiola, A. Ghribi, W. Holzapfel, A.T. Lee, X.F. Meng, M.J. Myers, R. O'Brient, E. Quealy, G. Rebeiz, P. Richards, D. Rosen, P. Siritanasak, Multi-chroic dual-polarization bolometric detectors for studies of the cosmic microwave background, in 23rd International Symposium on Space Terahertz Technology 2012, ISSTT 2012 1, pp. 55–61 (2012). https://doi.org/10.1117/12.924869
4. M.H. Abitbol, Z. Ahmed, D. Barron, R.B. Thakur, A.N. Bender, B.A. Benson, C.A. Bischoff, S.A. Bryan, J.E. Carlstrom, C.L. Chang, et al. Cmb-s4 technology book. arXiv preprint arXiv:1706.02464 (2017)
5. J.M. Geria, M.R. Hampel, S. Kempf, J.J.F. Bonaparte, L.P. Ferreyro, M.E.G. Redondo, D.A. Almela, J.M.S. Salum, N.A. Müller, J.D.B. Neira, A.E. Fuster, M. Platino, A. Etchegoyen, Suitability of magnetic microbolometers based on paramagnetic temperature sensors for CMB polarization measurements. J. Astron. Telesc. Instrum. Syst. **9**(1), 016002 (2023). https://doi.org/10.1117/1.JATIS.9.1.016002
6. C. Enss, A. Fleischmann, K. Horst, J. Schönefeld, J. Sollner, J.S. Adams, Y.H. Huang, Y.H. Kim, G.M. Seidel, J. Low Temp. Phys. **121**(3/4), 137–176 (2000). https://doi.org/10.1023/a:1004863823166
7. A. Fleischmann, L. Gastaldo, S. Kempf, A. Kirsch, A. Pabinger, C. Pies, J.P. Porst, P. Ranitzsch, S. Schäfer, F.V., Seggern, T. Wolf, C. Enss, G.M. Seidel, Metallic magnetic calorimeters, in AIP Conference Proceedings **1185**(1), 571–578 (2009). https://doi.org/10.1063/1.3292407

8. S. Kempf, A. Fleischmann, L. Gastaldo, C. Enss, Physics and applications of metallic magnetic calorimeters. J. Low Temp. Phys. **193**, 365–379 (2018). https://doi.org/10.1007/s10909-018-1891-6
9. J.-C. Hamilton, L. Mousset, E. Battistelli, P. De Bernardis, M.-A. Bigot-Sazy, P. Chanial, R. Charlassier, G. D'Alessandro, M. De Petris, M.G. Lerena, Qubic i: overview and science program. J. Cosmol. Astropart. Phys. **2022**(04), 034 (2022)
10. S. Kempf, M. Wegner, L. Deeg, A. Fleischmann, L. Gastaldo, F. Herrmann, D. Richter, C. Enss, Design, fabrication and characterization of a 64 pixel metallic magnetic calorimeter array with integrated, on-chip microwave squid multiplexer. Supercond. Sci. Technol. (2017). https://doi.org/10.1088/1361-6668/aa6d17
11. B. Dober, D.T. Becker, D.A. Bennett, S.A. Bryan, S.M. Duff, J.D. Gard, J.P. Hays-Wehle, G.C. Hilton, J. Hubmayr, J.A.B. Mates, C.D. Reintsema, L.R. Vale, J.N. Ullom, Microwave squid multiplexer demonstration for cosmic microwave background imagers. Appl. Phys. Lett. **111**, 1–11 (2017). https://doi.org/10.1063/1.5008527
12. ...B. Dober, Z. Ahmed, K. Arnold, D.T. Becker, D.A. Bennett, J.A. Connors, A. Cukierman, J.M. D'Ewart, S.M. Duff, J.E. Dusatko, J.C. Frisch, J.D. Gard, S.W. Henderson, R. Herbst, G.C. Hilton, J. Hubmayr, Y. Li, J.A.B. Mates, H. McCarrick, C.D. Reintsema, M. Silva-Feaver, L. Ruckman, J.N. Ullom, L.R. Vale, D.D.V. Winkle, J. Vasquez, Y. Wang, E. Young, C. Yu, K. Zheng, A microwave squid multiplexer optimized for bolometric applications. Appl. Phys. Lett. (2021). https://doi.org/10.1063/5.0033416
13. L. Ferreyro, M.G. Redondo, M. Hampel, A. Almela, A. Fuster, J. Salum, J. Geria, J. Bonaparte, J. Bonilla-Neira, N. Müller, N. Karcher, O. Sander, M. Platino, M. Weber, A. Etchegoyen, An implementation of a channelizer based on a Goertzel filter bank for the read-out of cryogenic sensors. J. Instrum. **18**, 5 (2023). https://doi.org/10.1088/1748-0221/18/06/P06009
14. J.M. Salum, T. Muscheid, A. Fuster, M.E.G. Redondo, M.R. Hampel, L.P. Ferreyro, J.M. Geria, J. Bonilla-Neira, N. Müller, J. Bonaparte, A. Almela, L.E. Ardila-Perez, M. Platino, O. Sander, M. Weber, Aliasing effect on flux ramp demodulation: nonlinearity in the microwave squid multiplexer. J. Low Temp. Phys. (2023). https://doi.org/10.1007/s10909-023-02993-z
15. P. Balchandani, R.H. Torii, R. Shile, Thin-film persistent current switch. IEEE Trans. Appl. Supercond. **15**(3), 3821–3826 (2005)
16. T.R. Stevenson, M.A. Balvin, S.R. Bandler, A.M. Devasia, P.C. Nagler, K. Ryu, S.J. Smith, W. Yoon, Magnetic calorimeter option for the lynx x-ray microcalorimeter. J. Astron. Telesc. Instrum. Syst. **18**, 035001–7 (2019)
17. A. Fleischmann, C. Enss, G. Seidel, Metallic magnetic calorimeters. Cryogenic particle detection, pp. 151–216 (2005)
18. J. Clarke, A.I. Braginski, *The SQUID Handbook. Fundamentals and Technology of SQUIDS and SQUID Systems*, vol. 1, 1st edn. (Wiley, New York, 2004)
19. R. O'Brient, J. Edwards, K. Arnold, G. Engargiola, W. Holzapfel, A.T. Lee, M. Myers, E. Quealy, G. Rebeiz, P. Richards, Sinuous antennas for cosmic microwave background polarimetry, in Millimeter and Submillimeter Detectors and Instrumentation for Astronomy IV, vol. 7020, pp. 404–414 (2008). SPIE
20. R. O'Brient, P. Ade, K. Arnold, J. Edwards, G. Engargiola, W. Holzapfel, A.T. Lee, X.-f. Meng, M. Myers, G. Rebeiz, Sinuous-antenna coupled tes bolometers for cosmic microwave background polarimetry, in AIP Conference Proceedings, vol. 1185, pp. 502–505 (2009). American Institute of Physics
21. A. Suzuki, K. Arnold, J. Edwards, G. Engargiola, W. Holzapfel, B. Keating, A.T. Lee, X.F. Meng, M.J. Myers, R. O'Brient, E. Quealy, G. Rebeiz, P.L. Richards, D. Rosen, P. Siritanasak, Multichroic dual-polarization bolometric detectors for studies of the cosmic microwave background. J. Low Temp. Phys. **176**(5–6), 650–656 (2014). https://doi.org/10.1007/s10909-013-1049-5
22. B. Westbrook, A. Cukierman, A. Lee, A. Suzuki, C. Raum, W. Holzapfel, Development of the next generation of multi-chroic antenna-coupled transition edge sensor detectors for cmb polarimetry. J. Low Temp. Phys. **184**, 74–81 (2016)
23. J.M. Edwards, R. O'Brient, A.T. Lee, G.M. Rebeiz, Dual-polarized sinuous antennas on extended hemispherical silicon lenses. IEEE Trans. Antennas Propag. **60**(9), 4082–4091 (2012). https://doi.org/10.1109/TAP.2012.2207048
24. D.P. McGinnis, J.B. Beyer, A broad-band microwave superconducting. IEEE Trans. Microwave Th. Techn. **36**(11), 1521–1525 (1988)
25. Z. Pourgholamhossein, G. Askari, H.M. Sadeghi, M. Fadaei, Analysis, design and simulation of a compact wide band vhf high power tubular band pass filter. Prog. Electromagn. Res. **967** (2014)

26. B. Westbrook, P. Ade, M. Aguilar, Y. Akiba, K. Arnold, C. Baccigalupi, D. Barron, D. Beck, S. Beckman, A. Bender, The polarbear-2 and simons array focal plane fabrication status. J. Low Temp. Phys. **193**, 758–770 (2018)
27. C.M. Posada, P.A.R. Ade, Z. Ahmed, A.J. Anderson, J.E. Austermann, J.S. Avva, R.B. Thakur, A.N. Bender, B.A. Benson, J.E. Carlstrom, F.W. Carter, T. Cecil, C.L. Chang, J.F. Cliche, A. Cukierman, E.V. Denison, T. Haan, J. Ding, R. Divan, M.A. Dobbs, D. Dutcher, W. Everett, A. Foster, R.N. Gannon, A. Gilbert, J.C. Groh, N.W. Halverson, A.H. Harke-Hosemann, N.L. Harrington, J.W. Henning, G.C. Hilton, W.L. Holzapfel, N. Huang, K.D. Irwin, O.B. Jeong, M. Jonas, T. Khaire, A.M. Kofman, M. Korman, D. Kubik, S. Kuhlmann, C.L. Kuo, A.T. Lee, A.E. Lowitz, S.S. Meyer, D. Michalik, C.S. Miller, J. Montgomery, A. Nadolski, T. Natoli, H. Nguyen, G.I. Noble, V. Novosad, S. Padin, Z. Pan, J. Pearson, A. Rahlin, J.E. Ruhl, L.J. Saunders, J.T. Sayre, I. Shirley, E. Shirokoff, G. Smecher, J.A. Sobrin, L. Stan, A.A. Stark, K.T. Story, A. Suzuki, Q.Y. Tang, K.L. Thompson, C. Tucker, L.R. Vale, K. Vanderlinde, J.D. Vieira, G. Wang, N. Whitehorn, V. Yefremenko, K.W. Yoon, M.R. Young, Fabrication of detector arrays for the spt-3g receiver. J. Low Temp. Phys. **193**, 703–711 (2018). https://doi.org/10.1007/s10909-018-1924-1
28. J. Aumont, S. Banfi, P. Battaglia, E. Battistelli, A. Bau, B. Bélier, D. Bennett, L. Bergé, J.P. Bernard, M. Bersanelli, et al. Qubic technical design report. arXiv preprint arXiv:1609.04372 (2016)
29. C. O'Sullivan, M. De Petris, G. Amico, E. Battistelli, P. De Bernardis, D. Burke, D. Buzi, C. Chapron, L. Conversi, G. D'Alessandro, Qubic viii: optical design and performance. J. Cosmol. Astropart. Phys. **2022**(04), 041 (2022)
30. P.L. Richards, Bolometers for infrared and millimeter waves. J. Appl. Phys. **76**(1), 1–24 (1994)
31. S.-Y. Kim, Generalized schottky anomaly. J. Korean Phys. Soc. **65**(7), 970–972 (2014)
32. M. Hampel, A. Almela, J. Bonaparte, J.B. Neira, L. Ferreyro, A. Fuster, M.G. Redondo, R. Gartmann, J. Geria, N. Müller, et al. The magnetic microbolometer: a proposal for qubic next gen (2023)